AGU PUBLICATIONS

JGR

Journal of Geophysical Research: Earth Surface

RESEARCH ARTICLE
10.1002/2014JF003186

Key Points:
- Soil evolution in aeolian landscapes differ from bedrock-weathering landscapes
- Armoring plays a major role in soil evolution in bedrock-weathering landscapes
- Aeolian landscapes show considerable spatial variability in soil depth and PSD

Correspondence to:
S. Cohen,
sagy.cohen@ua.edu

Citation:
Cohen, S., G. Willgoose, T. Svoray, G. Hancock, and S. Sela (2015), The effects of sediment transport, weathering, and aeolian mechanisms on soil evolution, *J. Geophys. Res. Earth Surf.*, *120*, 260–274, doi:10.1002/2014JF003186.

Received 22 APR 2014
Accepted 8 DEC 2014
Accepted article online 12 DEC 2014
Published online 20 FEB 2015

The effects of sediment transport, weathering, and aeolian mechanisms on soil evolution

Sagy Cohen[1], Garry Willgoose[2], Tal Svoray[3], Greg Hancock[4], and Shai Sela[3]

[1]Department of Geography, University of Alabama, Tuscaloosa, Alabama, USA, [2]School of Engineering, The University of Newcastle, Callaghan, New South Wales, Australia, [3]Department of Geography and Environmental Development, Ben-Gurion University of the Negev, Be'er Sheva, Israel, [4]School of Environmental and Life Sciences, The University of Newcastle, Callaghan, New South Wales, Australia

Abstract Aeolian-derived soils are found throughout the world. Soil evolution processes in aeolian-dominated landscapes differ from processes in bedrock-weathering landscapes by a number of key aspects including the lack of (1) soil production depth dependency, (2) surface armoring, and (3) grain size self-organization in the soil profile. We use here a soil evolution model (mARM5D) to study the differences between aeolian and bedrock-weathering-dominated landscapes by analyzing soil evolution on a hillslope under various aeolian and bedrock-soil supply settings subject to fluvial and diffusive sediment transport. The model simulates spatial and temporal variation in soil particle size distribution (PSD) and profile depth for each grid cell on the landscape, as a function of physical weathering, aeolian deposition, and diffusive and fluvial sediment transport. Our results indicate that surface armoring plays a major role in soil evolution. Under bedrock-weathering-dominated conditions, armoring reduces soil erosion and in conjunction with depth-dependent soil production, leads to steady state soil grading and depth and a relatively uniform soil distribution. In contrast, aeolian-dominated landscapes tend to have considerable spatial variability in soil depth and PSD. Our results also indicate that in contrast with diffusive transport, which is assumed to be PSD independent, fluvial sediment transport is strongly influenced by the soil production mechanism (aeolian or bedrock weathering). Based on the results presented here, we propose that aeolian-dominated landscapes are more responsive to environmental changes (e.g., climatic and anthropogenic) compared with bedrock-weathering landscapes. We further propose that this sensitivity may help explain the patchy soil distribution that is often observed in aeolian-dominated regions.

1. Introduction

Over geomorphological time scales, the production, transformation, and transport of soil through the landscape, generally referred to as soil evolution, is one of the predominant sets of processes affecting landscape characteristics [*McFadden and Knuepfer*, 1990; *Roering*, 2008]. Aeolian-derived soils are widespread throughout the world, e.g., the Huangtu Plateau in central China and the West European Loess Belt. However, unlike bedrock-weathering-dominated landscapes, which have been extensively studied in the literature [e.g., *Gilbert*, 1877; *Carson and Kirkby*, 1972; *Heimsath et al.*, 1997; *Vanwalleghem et al.*, 2013], our understanding of aeolian-derived soil evolution is still somewhat conceptual and qualitative in nature [*Hughes et al.*, 2009, 2010].

In this paper we compare aeolian and bedrock-weathering soil evolution. Other soil types (e.g., fluvial, lacustrine, deltaic, and marine), also likely to have some unique soil evolution dynamics, are beyond the scope of this study. From a soil evolution point of view, landscapes dominated by aeolian soil production (where soil material is transported to a given area from the outside) differ from bedrock-weathering-dominated landscapes in several ways. In bedrock-weathering systems, in situ weathering rates decrease exponentially (or close to exponentially, i.e., the "humped" soil production function; discussed later) with soil depth [*Gilbert*, 1877; *Ahnert*, 1977], thus regulating soil production as a function of regolith thickness [*Heimsath et al.*, 1997]. Weathering of regolith and soil leads to vertical trends in particle size distribution (PSD) within the soil profile with finer PSD closer to the surface as a function of the soil and regolith age, i.e., time exposed to weathering [*Yoo and Mudd*, 2008a]. At the soil surface, armoring can develop by size-selective entrainment which limits sediment transport by overland flow [*Willgoose and Sharmeen*, 2006; *Kim and Ivanov*, 2014]. Other surface attributes, such as vegetation shielding, may also lead to similar trends. Given sufficient time, these processes—depth-dependent

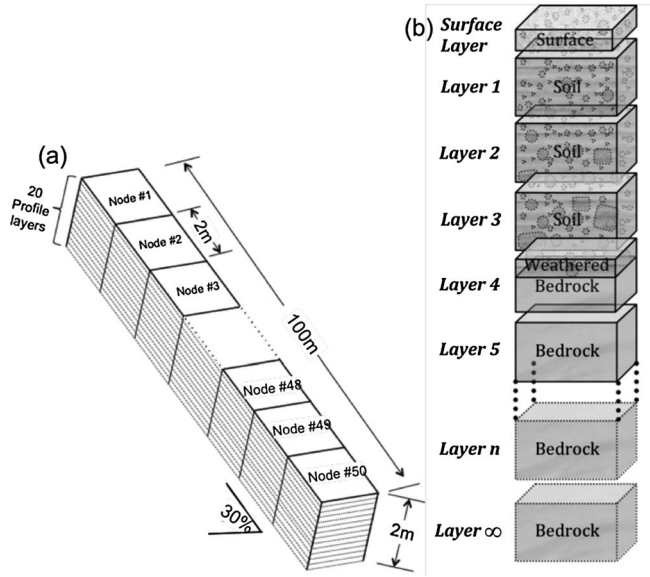

Figure 1. Schematics of the simulated domain: (a) 100 m linear hillslope divided into 50 2 × 2 m grid cells each with 20 profile layers and (b) soil profile in one grid cell, modified from *Cohen et al.* [2013].

weathering, vertical self-organization, and surface armoring—will stabilize the soil leading to steady state or dynamic equilibrium conditions [*Cohen et al.*, 2013].

In aeolian-dominated landscapes, the aforementioned controls on soil production and transport are not as prominent as (1) soil material is transported to the system from outside, i.e., no depth dependency on the soil production rate and (2) new material is continuously deposited on top of older surface soils which offsets the potential impact of surface armoring and vertical self-organization. In addition, aeolian-derived soils tend to have a finer PSD and are therefore potentially more erodible than bedrock-produced soils.

Identifying and quantifying the specific contribution of individual soil evolutionary processes and drivers are highly challenging. Numerical models of soil evolution are a particularly attractive research tool as they provide a virtual laboratory for isolating and testing different processes and drivers. Until now, aeolian input has been rarely incorporated into process-based models, rather calibrated against measured soil thickness at the field [e.g., *Crouvi et al.*, 2013; *Pelletier et al.*, 2011]. In this paper, instead of calibrating the model to a specific site, we present a conceptual study addressing the soil response to different evolutionary mechanisms derived from aeolian and weathering soil supply. We use a new spatially and temporally explicit numeric simulation model to investigate the differences between aeolian and weathering soil production and their response to sediment transport mechanisms. In a series of hillslope-scale simulations, we show the explicit effect and contribution of hillslope fluvial (rilling and hillslope wash) and diffusive (soil creep) sediment transport mechanisms on the soil and how these differ under aeolian and bedrock-weathering-dominated soil production regimes.

2. Methodology

2.1. The Model

We have developed in this paper a dynamic soil evolution model (mARM5D) to simulate soil physics as a state-space system as an extension of the mARM3D model [*Cohen et al.*, 2009, 2010]. The mARM5D is a modular and computationally efficient modeling platform that explicitly simulates three spatial dimensions in addition to a temporal dimension and a particle size dimension (hence the 5-D suffix). The model simulates soil evolution over a given landscape by describing changes in PSD in a finite number of equally thick soil profile layers (size and number defined by the user) in each grid cell (Figure 1).

The soil profile at a given grid cell is described as a vector of vectors, and the PSD is described for each layer in each grid cell with a PSD vector that quantifies the relative contribution of each particle size fraction per unit mass (e.g., Table 1). Vectors are used in mARM5D because they are a convenient and computationally efficient mathematical expression of change in soil grading. Loss in one size class necessarily means a relative enrichment in the remaining size classes and vice versa. Changes in PSD vectors are calculated with transition matrices that express the simulated processes (e.g., physical weathering). This model architecture provides superior computational efficiency and modularity [*Cohen et al.*, 2009]. Resulting from this unique modeling approach, most of the model's governing equations, described below, are different than the typical flux equations as they control the relative change in PSD vector in each profile layer in each grid cell. A full description of the mARM model architecture as a platform to mARM5D can be found in *Cohen et al.* [2009, 2010].

Table 1. Soil Grading Size-Class Diameters and the Initial Surface Particle Size Distribution[a]

Size-Class Diameter Lower Boundary (mm)	Material Retained (% per Unit Mass)
0.0	10
0.0013	3
0.003	3
0.0055	2
0.0085	3
0.015	3
0.02	2
0.065	2
0.075	1
0.15	1
0.425	0.5
0.75	1
2.36	8
5.0	23.5
7.5	4.75
9.375	4.75
11.25	4.75
13.125	4.75
15	7.5
17	7.5
19	1.5
22	1.5
>25	0

[a]For example, the smallest size class is between 0 and 0.0013 mm, and 10% of soil particles in the initial PSD falls within this diameter range. The largest class (particles larger than 25 mm) represents immobile bedrock in this study. The number and range of the size classes is user defined, allowing high degree of flexibility in the PSD classification (e.g., U.S. Department of Agriculture taxonomy). The PSD used in this study is based on *Cohen et al.* [2010].

In this study we simulate the spatial and temporal changes in PSD as resulting from (1) physical weathering of bedrock and soil particles in each profile layer, (2) aeolian deposition on top of the surface layer, (3) size-selective entrainment and deposition by overland flow (generally referred to here as fluvial sediment transport) from/on the surface layer, and (4) nonsize-selective diffusive sediment transport (creep) both on the surface and within the soil profile. Below, we provide a general description of how mARM5D evolves PSD and soil depth. The algorithms and governing equations for these processes are described in the subsections that follow.

In this study we assume that weathering changes the PSD of each soil-bearing profile layer by breaking down the soil particles, resulting in a finer PSD. The largest class in the PSD vector (>25 mm in this study; Table 1) represents bedrock. Bedrock weathering will enrich the smaller PSD vector classes at the expense of the bedrock class, generating soil particles. Soil particles are also subject to weathering which will result in a finer PSD over time. Both bedrock- and soil-weathering rates are assumed to be depth dependent.

Fluvial erosion will remove soil particles from the surface layer that are small enough to be entrained by the overland flow. As a result, the PSD of the surface layer will become coarser over time, which may lead to the development of an armor layer. Diffusive erosion is not considered to be particle size selective in this study (an outline of the main assumptions employed in this paper is provided in section 2.2). Each profile layer is considered to be perfectly mixed and so when soil is deposited to a layer by aeolian process or from an upstream grid cell (by fluvial or diffusive sediment transport), the transported sediment (at a given PSD) will mix with the existing soil particles. This will change the PSD of the receiving layer as a proportion of the mass of the deposited material relative to the mass of the soil in that layer. To illustrate this dynamic layer-mixing algorithm, let us look at an example of a simple algorithm that only calculates changes in the median PSD diameter (d_{50}): for a 1 m^3 profile layer with d_{50} of 10 mm, we deposit 0.1 m^3 of sediment with a d_{50} of 20 mm. The resulting d_{50} will be $(10 \times 0.9) + (20 \times 0.1) = 11$ mm. The mARM5D algorithm is more explicit as it calculates this relative change in PSD for each grading class (Table 1).

Changes in soil depth are simulated by explicitly tracking the vertical location of the soil-bedrock boundary in each grid cell. As the simulation begins, all the profile layers are occupied by bedrock. If weathering is simulated, bedrock will break into a smaller PSD class, which is considered to be soil/saprolite, thus lowering

the soil-bedrock interface layer (Figure 1b). Bedrock weathering will only occur at the layer that holds the soil-bedrock boundary. Erosion will remove soil from the surface resulting in decreasing soil depth (by "pushing" the soil-bedrock interface upward). Deposition in a grid cell, either by aeolian sediment supply or by sediment transport from an upstream grid cell, will result in an increasing soil depth. Deposition pushes material from a profile layer into the layer below which in turn pushes material into the layer below and eventually ending at the layer with the bedrock-soil interface, where the final result is to push the bedrock-soil interface deeper down the profile.

As outlined in section 2.2 below, one of the assumptions employed in this paper is that changes in soil depth and PSD will not affect the topography and thus the slopes and contributing areas of the simulated landscape (i.e., no explicit landform evolution). In addition, while the model can explicitly incorporate biological (e.g., bioturbation) and chemical (e.g., chemical weathering) processes [*Cohen et al.*, 2010], these are neglected at this stage for the sake of simplicity.

2.1.1. Fluvial Sediment Transport

For each grid cell, the top layer is the surface layer exposed directly to size-selective erosion (Figure 1). Sediment transport capacity over a time step (q_s, m^3/m) at the surface is calculated by a modified *Engelhund and Hansen* [1968] equation:

$$q_s = e\frac{q^{n_1}S^{n_2}}{(1-s)^2 {d_{50}}^{n_3}}\Delta t \tag{1}$$

where e is an empirical erodibility factor; q is the discharge per unit width ($m^3/s/m$); S is the slope; d_{50} is the median diameter (m) of the material in the surface layer; s is the specific gravity of sediment ($s = 2.65$; kg/m^3); n_1, n_2, and n_3 are calibration parameters; and Δt is the time step size. The units of erodibility parameter e are a function of the calibration exponents n_1, n_2, and n_3 and are defined such that the units of q_s are the ones specified. Here we use $n_1 = 1$ and $n_2 = 1.2$ based on a calibration in *Cohen et al.* [2009] and modified n_3 to 0.5 (from 0.025) to adjust for the very fine grained aeolian sediment.

Discharge (q; $m^3/s/m$) is

$$q = \left[\frac{A}{A_p}\right]^{n_4}\frac{Q}{(A_p)^{0.5}} \tag{2}$$

where Q (m^3/s) is the excess hillslope runoff variable (discussed later), A is the upslope contributing area (m^2), A_p is the area of a grid cell unit (m^2), and n_4 is a constant relating runoff as a function of the contributing area. We assume a linear relationship between contributing area and runoff discharge ($n_4 = 1$). Water is routed to a neighboring grid cell with the "steepest descent" (D8) algorithm [*O'Callaghan and Mark*, 1984].

Erosion (E) is the difference between inflowing and outflowing sediment discharge in a grid cell in each time step:

$$E = \Delta q_s = q_s - \sum q_{sUS} \tag{3}$$

where Σq_{sUS} is the sum of the sediment discharge from the adjacent grid cells draining into that grid cell and q_s is the sediment discharge out of the grid cell. For $E > 0$, erosion is calculated with size-selective entrainment of fine material from the surface (underscore is a vector notation in this paper)

$$h_s \underline{g_s}_{t+1} = h_s \underline{g_s}_t - \underline{G} \tag{4a}$$

$$\text{where } G_i = E\Delta t \begin{cases} \frac{a}{d_i} g_{si} & \text{for } i < M \\ b\frac{a}{d_i} g_{si} & \text{for } i = M \\ 0 & \text{for } i > M \end{cases} \tag{4b}$$

where $\underline{g_s}^t$ is the vector for the surface layer PSD (e.g., Table 1) at time t, d_i is the mean diameter (m) of PSD size class i, a and b are the scaling factors, M is a size threshold that determines the largest particle diameter that can be entrained in the flow as determined by Shield's shear stress threshold (size classes with particle diameter smaller or equal to M will be subject to erosion), and h_s is the thickness of the surface layer. Vector $\underline{G}$ is the change in the grading of the i size classes in time step Δt, and g_{si} is the value of the ith entry in the grading vector $\underline{g_s}_t$. The sediment diameter dependency in equation (4b) is such that the erosion process

preferentially removes the finer material from the surface, resulting eventually, in the absence of other processes, in an immobile surface armor of coarse particles. If the mass of erosion is larger than that of the surface layer, soil will be eroded from the profile layer below it.

Since mARM5D is a mass balance model and the mass of the layers is constant with time (Figure 1), an amount of sediment equal to the eroded mass is resupplied to the surface layer from the top profile layer (*Layer 1*; Figure 1b). The top profile layer (*Layer 1*) is then resupplied by the layer directly below, *Layer 2*, and so on until the bottom layer *n*. Layer *n* is resupplied from the semiinfinite bottom layer (*Layer* ∞), which for a natural soil profile we consider to be bedrock. This is how the soil profile evolves.

For $E < 0$, deposition per time step is

$$h_s \underline{g}_{s_{t+1}} = h_s \underline{g}_{s_t} - E\, \underline{g}_f\, V_s\, \Delta t \tag{5}$$

where $\underline{g}_f$ is the grading distribution of the sediment suspended in the overland flow at time t and V_s is the settling velocity (e.g., calculated based on Stokes' law [*Henderson*, 1966]) for each size class as a function of its mean diameter. The profile evolution is such that an amount of sediment equal to the deposited mass is supplied to the first top profile layer (*Layer 1*; Figure 1b) from the surface layer. The top profile layer (*Layer 1*) then supplies the same mass of sediment to the layer directly below, *Layer 2*, and so on until the bottom layer *n*, which "pushes" the soil-bedrock boundary down the profile (Figure 1b).

2.1.2. Diffusive Sediment Transport

Traditionally, equations of two-dimensional diffusive transport calculate sediment discharge as a linear relationship to slope, soil thickness, and a diffusion coefficient (e.g., the creep model of *Culling* [1963] or the viscous flow model of *Ahnert* [1976]), and if the soil is explicitly modeled at all, diffusion is considered independent of depth through the profile. Simulation of the soil profile in mARM5D is novel as it explicitly calculates diffusive transport for each soil profile layer. Based on *Roering* [2004], the diffusivity is assumed to decrease exponentially with depth below the soil surface:

$$D_l = D_s[\exp(-\lambda h_l)] \tag{6}$$

where D_l (m/yr) is the diffusive transport rate for the layer l, D_s is the surface (maximum) diffusive sediment transport rate (m/yr), h_l is the mean depth (m) of profile layer l relative to the surface, and λ is a calibration parameter. Here we use $\lambda = 0.02$ based on *Fleming and Johnson* [1975] and *Roering* [2004]. The surface diffusion sediment transport rate (D_s; m/yr) is

$$D_s = S^{\beta} k \Delta t \tag{7}$$

where k is the surface diffusivity. Here as in most studies, we assume a linear relationship with slope ($\beta = 1.0$). Sediment flux for each layer can be calculated by multiplying D_s by the volume and the bulk density of the soil. We assume here constant volume and bulk density. This assumption will be further discussed later in this paper.

The sediment transported from each profile layer is added to an equivalent layer at the grid cell downslope (e.g., 10 g of soil from *Layer* 2 in grid cell *i* will be added to *Layer* 2 in the downslope grid cell). If that downslope layer is completely occupied by bedrock, the sediment is added to the soil-bedrock boundary layer (pushing it downward). Consider for example when the bedrock/soil boundary at time step t is in layer #10 (100 cm below the surface) in grid cell x and layer #5 (50 cm) in x_{ds} (its downstream grid cell). Sediment transported from layers #1–5 in grid cell x through diffusive processes will be added to their equivalent layers (#1–5) in grid cell x_{ds}. Sediment transported from layers 6–10 in grid cell x through diffusive processes will be added to layer #5 in pixel x_{ds}, pushing the bedrock/soil boundary downward.

Equations (6) and (7) mean that the mass of soil transported by diffusive processes will increase nonlinearly as a function of available soil; i.e., a greater soil thickness in a given grid cell will result in greater sediment transport by diffusion. This nonlinearity means that while deeper soil profiles will yield an overall greater diffusive transport mass, increase in soil depth will not result in a linear increase in soil transport. This stems from equation (6) that dictate that deeper profile layers will have an exponentially declining transport rate.

2.1.3. Weathering

The profile layers are subject to bedrock and soil weathering (Figure 1b). Here we consider physical weathering calculated by breaking a parent particle into two daughter particles. As mass conservation is

assumed, the diameters of the daughter particles (d_1 and d_2) can be determined from the diameter of the parent particle (d_0):

$$d_1 = \frac{d_0}{(1+n^3)^{1/3}}; d_2 = \frac{d_0}{(1+(1+n^3))^{1/3}} \quad (8)$$

where n is the geometry of the particle breakdown (the ratio between a daughter particle and its parent particle). Based on experimental studies presented by *Wells et al.* [2008], we used a split-in-half geometry, where $n = 0.5$, which leads to $d_1 = d_2$.

A bedrock- and soil-weathering depth-dependent equation is used to set the weathering rate in each profile layer as a function of its depth below to the surface [*Heimsath et al.*, 1997]. Based on *Cohen et al.* [2010], we used a modified version of the humped soil production function [*Ahnert*, 1977] proposed by *Minasny and McBratney* [2006]:

$$W_l = P_0[\exp(-\delta_1 h_1 + P_a) - \exp(-\delta_1 h_1)] \quad (9)$$

where W_l is the physical weathering rate for profile layer l; P_0 and P_a (mm/yr) are the potential (or maximum) and steady state weathering rates, respectively; h_l (m) is the depth below the surface for layer l; and δ_1 and δ_2 are the constants. The values proposed by *Minasny and McBratney* [2006] of $\delta_1 = 4$, $\delta_2 = 6$, $P_a = 0.005$ mm/yr are used here.

2.1.4. Aeolian Deposition

Sediment, with a user-defined grading distribution ($\underline{g_a}$), is added to the surface layer. The aeolian deposition rate (K_a; mm/yr) is assumed to be spatially uniform:

$$h_s \underline{g_s}_{t+1} = h_s \underline{g_s}_t + K_a \underline{g}_a \quad (10)$$

For the sake of simplicity, aeolian sediment is assumed to originate from outside the system, and no aeolian erosion is considered within the simulated domain. This means that K_a is, in our case, the aeolian sediment accumulation (deposition) rate.

2.2. Boundary Conditions

Although mARM5D is a landscape-scale model, we base our analysis in this paper on a synthetic hillslope with a constant (linear) slope (Figure 1a). This allows us to more easily identify causality and trends that may get obscured in a complex landscape-scale simulation. The hillslope is one grid cell in width and 50 in length (downslope) with 20 profile layers overlain by a thin surface layer in each grid cell (Figure 1). Each grid cell is 2×2 m, each profile layer is 10 cm in thickness, and the surface layer is 0.5 cm in thickness. All simulations were run for 80,000 years to ensure that steady state conditions were reached (constant soil depth and PSD). At the start of the simulation, only the surface layer contains soil (initial PSD described in Table 1), while the soil layers below are initially entirely bedrock.

2.3. Assumptions

Soil evolution is highly complex, combining a multitude of chemical, biological, and mechanical processes with highly heterogeneous temporal and spatial dynamics [*Hillel*, 1982]. Numerical models are inherently a simplified expression of reality, and while we can simulate many different processes and drivers in our model, we chose to focus on a narrow set of soil evolution dynamics. This allows us to isolate and quantify the specific impact of individual process and driver. While this is advantageous for this kind of conceptual study, it complicates the extrapolation of the results to "real" landscapes. This is because processes and drivers that were not explicitly simulated may alter the results in unknown ways. Below, we outline the main assumptions made here. The implications of these are analyzed in the Discussion section.

Topography–we assume a spatially constant topographic slope that, as in our previous studies of soil evolution [e.g., *Cohen et al.*, 2009, 2010, 2013; *Willgoose and Sharmeen*, 2006], does not change during the simulation (i.e., topographic uplift rate is assumed equal to erosion rate [*Cohen et al.*, 2009]).
Soil profile PSD–each soil profile layer has the same volume and is considered to be perfectly mixed. This limits the vertical representation of PSD variability in favor of algorithmic simplicity because it significantly lowers simulation run time. No biological or chemical processes (e.g., bioturbation and leaching) are simulated.

Table 2. Simulation Description and Parameterization

Simulation	Description	Aeolian Deposition Rate (mm/yr)	Weathering Potential Rate (mm/yr)	Runoff Discharge (m^3/yr)	Surface Diffusivity (mm/yr)
1. S_{WF}	Weathering with fluvial sediment transport	0.0	0.1	1.705×10^{-4}	0.0
2. S_{WD}	Weathering with diffusive sediment transport	0.0	0.1	0.0	10.075
3. S_{WC}	Weathering with combined fluvial and diffusive transport	0.0	0.1	6.6×10^{-5}	6.0
4. S_{cAC}	Coarse aeolian with combined fluvial and diffusive transport	0.1	0.0	6.6×10^{-5}	6.0
5. S_{cAWC}	Coarse aeolian and weathering with combined fluvial and diffusive transport	0.05	0.05	6.6×10^{-5}	6.0
6. S_{fAWC}	Fine aeolian and weathering with combined fluvial and diffusive transport	0.05	0.05	6.6×10^{-5}	6.0

Soil hydrology–changes in soil water infiltration rates or water holding capacity are not simulated, and so the explicit effects of soil profile PSD, e.g., bulk density, or chemical properties, e.g., clay formation, are not taken into account.

Soil geomorphology–entrainment potential of soil surface is simulated as a function of particle diameter. It does not take into account the potential chemical properties like the formation of aggregates in clay soils. The diffusion transport process is not particle size selective.

Climatic and anthropogenic drivers–interannual and intraannual precipitation is assumed constant throughout the simulations. Anthropogenic or any other environmental factors (e.g., grazing fire) are not considered.

Soil production–two soil production mechanisms are considered: physical weathering and aeolian deposition. Chemical and biological weathering processes and agents are not simulated.

Aeolian transport–aeolian soil production is assumed to be the net between aeolian deposition and erosion which is simulated as constant in space and time.

2.4. Simulation Settings

2.4.1. Simulation Scenarios

The effect of slope gradient on the results is examined in a sensitivity analysis in which we compare four simulations with four different slope gradients (5, 10, 15, and 30%). Following the slope sensitivity analysis, we compare six simulations that employ different soil production (physical weathering and/or aeolian deposition) and sediment transport mechanisms (fluvial and/or diffusive) according to the following characteristics (Table 2):

1. S_{WF} – *Weathering* with *Fluvial* sediment transport,
2. S_{WD} – *Weathering* with *Diffusive* sediment transport,
3. S_{WC} – *Weathering* with *Combined* fluvial and diffusive sediment transport,
4. S_{cAC} – *Coarse*-grained *Aeolian* deposition with *Combined* fluvial and diffusive sediment transport,
5. S_{cAWC} – *Coarse*-grained *Aeolian* deposition and *Weathering* with *Combined* fluvial and diffusive sediment transport, and
6. S_{fAWC} – *Fine*-grained *Aeolian* deposition and *Weathering* with *Combined* fluvial and diffusive sediment transport.

Simulations #1 and #2, employing either the fluvial or diffusive sediment transport (S_{WF} and S_{WD}, respectively), explore the contribution of each transport mechanism to soil evolution and the effect of surface armoring. Diffusive processes in this model are not particle size selective and therefore, unlike the modeled fluvial transport, will not lead to surface armoring.

Simulations #3 and #4 explore the effect of soil production depth dependency. In simulation #3, soil production is only through weathering (S_{WC}) and is therefore depth dependent, while in simulation #4, soil is aeolian, and so it is deposited on the surface at a constant rate. To isolate the effects of differences in PSD, the aeolian-deposited sediment in simulation #4 (S_{cAC}) is coarse grained ($d_{50} = 6.117$ mm), equal to the initial surface PSD used in all the simulations in this paper (Table 1).

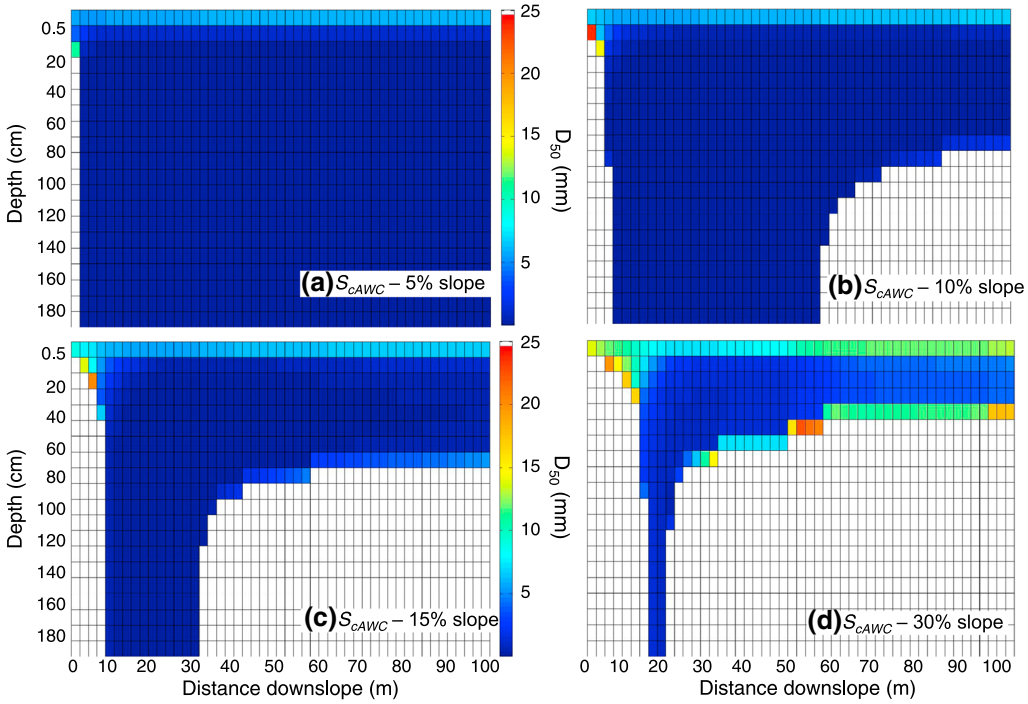

Figure 2. Sensitivity analysis results showing d_{50} (color gradient) at the end of the simulation for each profile layer (y axis) along the hillslope (x axis) at slope gradients of (a) 5%, (b) 10%, (c) 15%, and (d) 30%.

Simulations #5 and #6 explore the effects of aeolian PSD by employing a realistic fine-grained aeolian PSD ($d_{50} = 0.06$ mm) in combination with bedrock weathering (S_{fAWC}) and comparing it to a similar simulation (S_{cAWC}) but with coarse-grained aeolian PSD ($d_{50} = 6.117$ mm).

2.4.2. Model Parameterization

Fitting parameter values is challenging for complex, physically based models. Parameters are usually based on previous studies or various calibration processes, e.g., Monte Carlo simulations, field or laboratory-based experiments. Most of the mARM5D coefficients were adopted from our previous studies with mARM, as described in section 2.1 above. Here we compare simulations with different combinations of sediment transport and soil production mechanisms. As described below, our parameterization is primarily set to ensure comparability between the simulations.

The aeolian deposition rate (K_a in equation (10)) was based on published values near the Lehavim LTER (Long-Term Ecological Research) and was set to 0.1 mm/yr [*Bruins and Yaalon*, 1992]. The Lehavim LTER is a semiarid and Loess-dominated field site in the northern Negev in Israel (31°20′N, 34°45′E; described in *Sela et al.* [2012]). While this field site is not the focus of the synthetic study presented here, we use these values as a subsequent study by the authors will examine the effects of climatic and anthropogenic drivers on the Lehavim LTER landscape-scale soil evolution. We matched the weathering rate potential (P_0 in equation (9)) to the aeolian deposition rate (0.1 mm/yr). In simulations that employ both aeolian deposition and weathering (e.g., S_{cAWC}), the total soil production rate was kept at 0.1 mm/yr by reducing aeolian deposition and weathering rate potential in half (0.05 + 0.05 mm/yr). This is again to ensure that these simulations are comparable to all other simulations.

In simulations that combine both fluvial and diffusive sediment transport mechanisms (e.g., S_{WC}), Q (equation (2)) was set to 6.6×10^{-5} m^3/yr based on *Eldridge et al.* [2002] and *Yair and Kossovsky* [2002]. The k parameter (equation (7)) was set to 6.0 mm/yr based on *Carson and Kirkby* [1972]. The low Q value is assigned as a result of the arid climatic conditions of Lehavim LTER site. While the value of Q is important for site-specific soil evolution dynamics, it is much less so in this comparative study. For simulations that employ only one transport mechanism (e.g., S_{WF} and S_{WD}, respectively), these two parameters cannot just be multiplied by a factor of 2 (as was the case for the soil production mechanisms). This is because these

parameters only control a portion of the overall sediment transport mechanism (runoff discharge and surface creep, respectively). The parameters were therefore adjusted based on a sensitivity analysis that matched the overall soil erosion by each transport mechanism. For the fluvial-only simulation, Q is set to 1.705×10^{-4} m^3/yr and $k = 0$. For the diffusive-only simulations, k is set to 10.075 mm/yr and $Q = 0$ (Table 2).

3. Results

3.1. Slope Sensitivity Analysis

Figure 2 (and the figures following it) shows steady state soil grading distributions down the hillslope (x axis) in each profile layer (y axis). The color gradient displays the median particle size diameter (d_{50}) with warm colors (high d_{50}) representing coarse PSD. Note that (1) the thin surface layer is plotted as having the same thickness as the underlying profile layers, (2) the white color represent the bedrock, and (3) the y and x axes are at different scales (centimeters and meters, respectively). Also, note that the topographic gradient of the simulated hillslope, declining elevation from left to right, is not illustrated in these plots.

Four slope gradients are compared (using the S_{cAWC} simulation settings; section 2.3.1): 5, 10, 15, and 30%. The lowest, 5%, slope has resulted in a soil profile which is almost completely occupied by very fine soils (Figure 2a). This is the result of a sediment transport rate, both fluvial and diffusive, being significantly lower than the soil production rates (combined aeolian deposition and bedrock weathering), and so soil depth reaches the maximum 2 m profile depth limit we used in this study, and a low-flow shear stress resulted in finer soil particles remaining on the surface. For steeper, 10 and 15%, slopes, there is a trend of increasing soil depth from the bottom of the hillslope to its intermediate section (from right to left in Figures 2b and 2c) with the upper section of the hillslope still reaching the 2 m soil depth limit. The size of this maximum soil depth section is inversely related to the slope (e.g., from Figures 2b to 2c) due to increasing sediment transport rate. The uppermost section of the hillslope (left side of each plot) has the lowest soil depth. The size of that low-depth section increases with increasing slope (e.g., from Figures 2b to 2c) due to increasing diffusion rates. The drivers leading to these somewhat counterintuitive soil distribution trends are discussed in the Discussion section.

The 5, 10, and 15% slope gradient simulations (Figures 2a–2c) resulted almost exclusively in fine-grained soils throughout the hillslope. In contrast, the 30% slope gradient simulation (Figure 2d), has resulted in a very distinct coarse grained surface (i.e., armor) and a coarse-grain bedrock-soil boundary. These differences in soil grading distribution are due to differences in the dominant soil supply mechanism: whereas low slopes (and thus low erosion) allow extensive accumulation of aeolian supplied sediment, it is limited under the condition of the steep 30% slope gradient. This steep slope gradient allows improved differentiation between the effects of both the aeolian and weathering soil production mechanisms, which are completely obscured by high aeolian accumulation rates at the low slope simulations. Consequently, the 30% slope gradient is applied in our analysis below.

It should be noted that results similar to the 30% simulation could be reached for low-slope simulation by adjusting the model's transport and soil production parameters (e.g., by lowering the aeolian deposition rate). The model parameterization is however based on our previous studies at the Lehavim LTER field site (which includes similarly steep slopes), rendering the 30% slope gradient as most suitable to the simulation settings used in this study.

3.2. Hillslope Simulations

Fluvial sediment transport under weathering-only soil production (S_{WF}) resulted in increasingly coarse surface grading down the hillslope (Figure 3a). This is due to increasing water discharge with contributing area downslope that allows for entrainment of larger soil particles by overland flow. The vertical soil profile PSD is a coarse layer, over a fine layer, over another coarse layer; the armor layer over weathered soil over regolith (or unweathered soil). Even though the transport capacity of the overland flow increases downslope (resulting in the coarser surface) soil depth only slightly decreases downslope (30 cm over the 100 m long hillslope). This is because armoring reduces the erosion rate at the bottom of the hillslope. This source-limited steady state soil distribution is in stark contrast to the diffusive simulation (S_{WD}; Figure 3b) that resulted in very thin and coarse soils at the top of the hillslope and thick and fine-grained soils at the bottom. The diffusive simulation soil distribution can be attributed to the fact that diffusion rate is not a function of

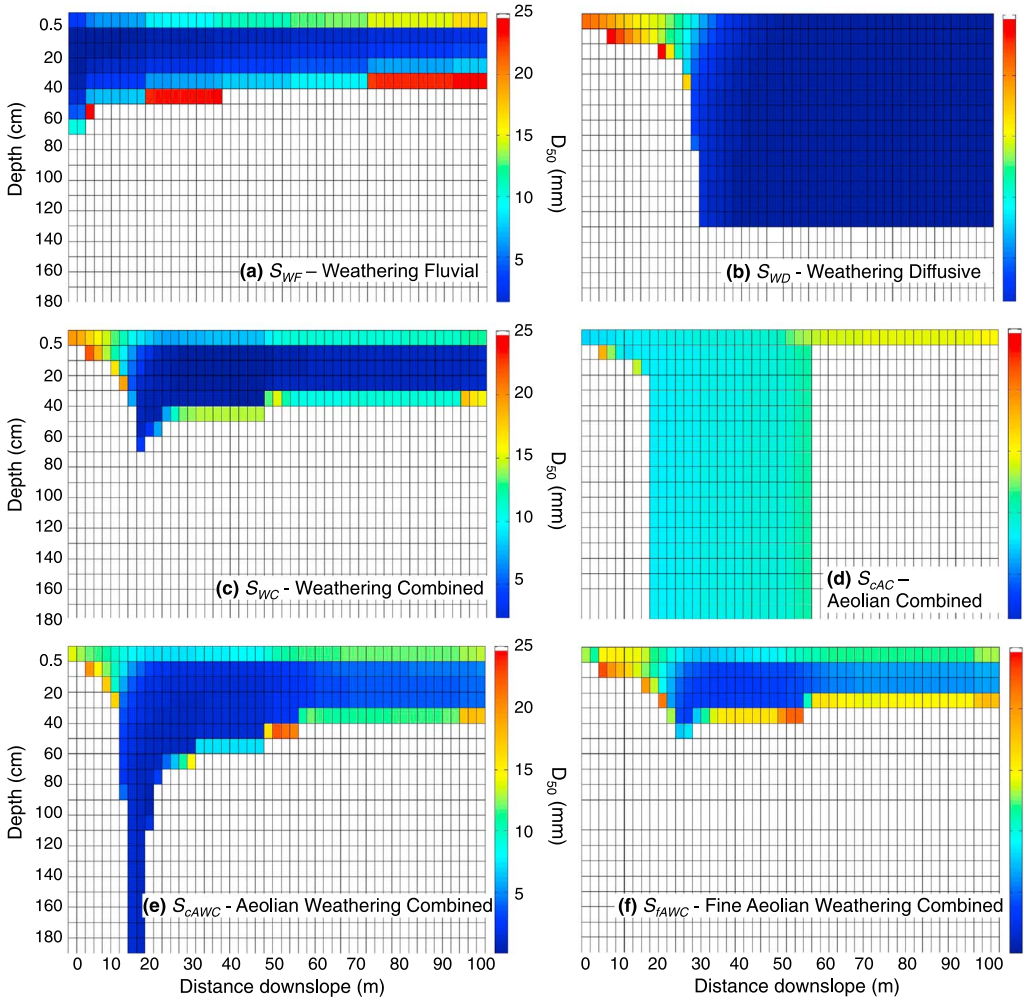

Figure 3. Soil grading distribution showing d_{50} (color gradient) for each profile layer (*y* axis) along the hillslope (*x* axis) at the end of simulation (a) S_{WF}, (b) S_{WD}, (c) S_{WC}, (d) S_{cAC}, (e) S_{cAWC}, and (f) S_{fAWC}, where *W*–weathering, *F*–fluvial, *D*–diffusion, *C*–combined fluvial and diffusive, *cA*–coarse-grained aeolian, and *fA*–fine-grained aeolian.

contributing area but of slope, which is spatially uniform in these simulations. Soil produced on the upper part of the hillslope is transported and accumulates at its lower section. The thick soil layer at the bottom of the hillslope considerably reduces bedrock weathering leading to a transport-limited steady state which differs considerably from the fluvial-driven steady state in S_{WF} (Figure 3a).

Combining both fluvial and diffusive sediment transport processes (S_{WC}) has resulted in a spatial soil distribution (Figure 3c) that is similar to the S_{WD} distribution (Figure 3b) at the top of the hillslope, where diffusion is the dominant transport mechanism, and a constant coarse over fine over coarse vertical soil distribution for the lower section of the hillslope where fluvial transport is dominant. A transition zone between the diffusive-dominated upper section and fluvial-dominated middle to lower section can be seen at about 20 m down the hillslope in Figure 3c. This section has the deepest soil profile and finest surface grading. It is formed by soil deposition from the upper hillslope section combined with relatively low runoff discharge (low fluvial erosion rate). For the lower section of the hillslope, surface armoring is less developed in S_{WC} than the S_{WF} simulation (Figure 3a) due to lower water discharge in this simulation. This is the outcome of the reduction in transport rate when both diffusive and fluvial sediment transport were considered, made to ensure that all the simulations have the same overall erosion rate (see section 2.4.2).

When soil supply is independent of depth (i.e., aeolian), but still has relatively coarse PSD (S_{cAC}; Figure 3d), the resulting soil distribution is very different from depth-dependent weathering soil evolution (S_{WC}; Figure 3c).

The upper section of the hillslope shows a gradual increase in soil depth followed by a section of deep soils, a sign of a diffusive-dominated sediment transport. At about midslope, soil depth decreases abruptly to near zero, with only the thin surface layer containing soil. This spatial trend is due to a shift from diffusive to fluvial-dominant sediment transport mechanism at the bottom part of the hillslope—also seen in the former results above (Figure 3c). The sharp transition in soil depth (from 200 to 0.5 cm in one grid cell) is caused by threshold-driven dynamics: when the runoff shear stress is high enough to entrain the aeolian-deposited sediment, almost all of the soil is eroded as aeolian sediment supply does not contain the coarse immobile fractions that are needed to form a surface armor.

When a very fine aeolian PSD is simulated as the only sediment supply mechanism, soil is almost completely eroded from the hillslope, leaving a soil-depleted hillslope with a few patches of very shallow fine-grained soil (the results of this simulation are not presented). This, and the results of the S_{cAC} simulation (Figure 3d), may help explain the patchy soil that is often observed in aeolian-dominated regions.

For the coarse aeolian combined with bedrock-weathering simulations (S_{cAWC}; Figure 3e), the resulting soil distribution is similar to the S_{WC} simulation but with deeper soils at the upper section of the hillslope. This increase in soil volume is due to larger sediment flux from aeolian deposition. Even though the aeolian and weathering soil production rates were adjusted (each cut in half) to allow this comparison, the lack of depth dependency in aeolian soil production translates to greater soil production over time. The footslope section of the hillslope is nearly identical to S_{WC} because the deposited aeolian sediment in S_{cAWC} is readily eroded from the surface.

When the S_{cAWC} simulation is repeated with a more realistic, fine-grained, aeolian sediment (S_{fAWC}), the resulting soil distribution (Figure 3f) is thinner in depth with a slightly coarser PSD, but overall, it is similar to the S_{WC} distribution (Figure 3c). The hump-shaped section is shallower and located a few meters downslope compared to the S_{WC} and S_{cAWC} simulations (Figures 3c and 3e, respectively). These differences are almost exclusively due to the lower weathering rate simulated in S_{fAWC}. The lack of an apparent aeolian signal in the resulting soil indicate that under these specific simulation configurations, input from fine-grained aeolian sediment has nearly no effect on long-term soil evolution.

4. Discussion

We have shown here that surface armoring and profile weathering lead to a distinct soil profile of two coarse layers which are separated by a fine material layer (e.g., Figures 3a and 3c). This profile leads to dynamic equilibrium in which soil production by bedrock weathering is balanced by surface erosion; for every soil particle produced at the soil-bedrock boundary, an equivalent mass of soil will weather to a size which is small enough to be entrained by overland flow, i.e., source-limited sediment transport regime [*Sharmeen and Willgoose*, 2006]. Surface PSD will vary in space as a function of overland flow characteristics. On a linear hillslope, increasing discharge downslope will result in a coarser surface. However, despite the increasing runoff shear stress and transport capacity downslope, soil depth remains fairly constant because the coarse surface materials (i.e., armor) offset this increase.

The formation of an armor layer emerges as a major stabilizing factor in the soil evolution process. This soil property can be affected by seasonal and long-term changes in flow characteristics. For example, a region dominated by short and intense storms might yield a different soil distribution compared to a region with more moderate but longer rain events. Longer-term changes in flow and land use characteristics in response to climate and anthropogenic changes can also affect soil distribution as they can alter the balance between soil production and erosion, among other processes and factors. For example, an increase in storm intensity or change in cultivation practices can destroy the surface armor, considerably altering the steady state soil distribution. These variations in precipitation and anthropogenic input will be the foci of a subsequent study.

Aeolian-sourced soils experience different soil dynamics than soils derived from bedrock weathering. In the absence of a depth-dependent soil production and surface armoring, equilibrium soil depth for aeolian soils is mainly a function of flow transport capacity. With an increasing transport capacity as a result of increasing flow discharge downslope, soil depth will change sharply from deep soil upslope to very thin soils downslope (Figures 3d and 4a). The results show that in the absence of other processes, e.g., weathering and diffusion (Figures 3e and 4b), the transition from deposition to erosion-dominated region will be sharp as it is controlled by a threshold dynamics; either the flow velocity in a given grid cell is high enough to entrain

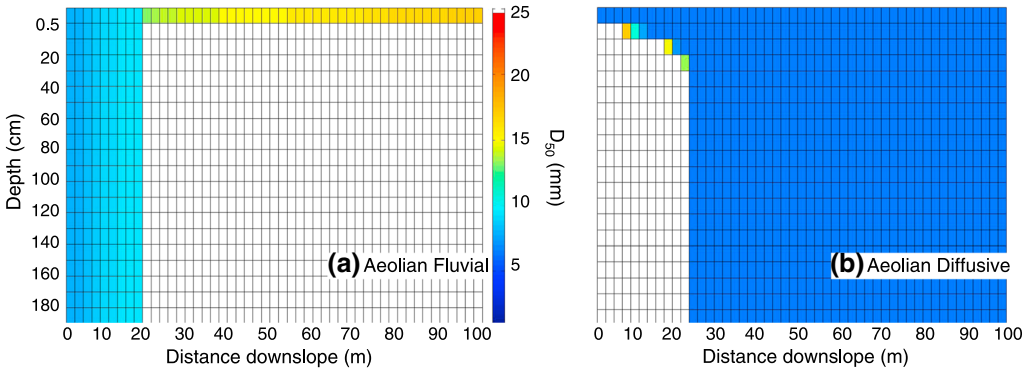

Figure 4. Soil grading distribution showing d_{50} (color gradient) for each profile layer (y axis) along the hillslope (x axis) at the end of simulation (a) aeolian with fluvial transport and (b) aeolian with diffusive transport.

the aeolian-deposited sediment or it is not. In practice, this is probably more complex; however, this suggests that aeolian-dominated regions are considerably more responsive (sensitive) to spatial and temporal changes in flow and land use dynamics compared to weathering-dominated regions.

For fine-grained aeolian input, all the deposited sediment was readily eroded from the hillslope. This is due to the fact that the fine aeolian sediment is readily entrained and transported by fluvial processes after it is deposited on the surface. This suggests that in order for loess soils to accumulate on the hillslopes, they need to be (1) shielded (e.g., by vegetation) from runoff shear stress, (2) subject to much lower runoff shear stress, or (3) deposited at higher rates than removal by fluvial transport.

Diffusive sediment transport was modeled as a function of local slope (equation (7)). This means that diffusive sediment transport in mARM5D is not affected by PSD or surface processes. This is a simplification of field observations as, for example, clay-rich soils tend to move more in response to wetting and drying cycles, while sand-rich soils are more strongly affected by raindrop impact saltation. Diffusive transport is simulated for each profile layer (with exponentially decreasing transport rate with depth under the surface; equation (6)) resulting in an overall increasing soil transport from one grid cell to its downslope neighbor with increasing soil depth. The results of the diffusive-driven simulations (Figures 3b and 4b) suggest that (1) diffusive processes are a potential driver of the "downslope thickening" soil distribution, commonly observed in soil-mantled hillslopes [*Pelletier*, 2008] and (2) differences in soil evolution between aeolian and weathering-dominated landscapes can be primarily attributed to surface armoring (or other forms of shielding) processes. The first point is well established in the literature [e.g., *Roering*, 2008]; however, this is the first time (to the best of our knowledge) it has been demonstrated in an explicit soil simulation.

The combination of both fluvial and diffusive sediment transport leads to a distinct soil distribution, a horizontal hump-shaped soil depth distribution (not to be confused with the vertical "hump" soil production equation) (Figures 2c–2f). This hump is the result of the transition from diffusive to fluvial-dominated sections of the hillslope. Its location and depth will therefore reflect the relative rates of the two processes. If the relative rates change in space and/or time, e.g., increase in overland flow in less-vegetated hillslopes or in response to increased precipitation, the soil distribution will be affected. *Cohen et al.* [2013] showed that soil response to climate fluctuations varies considerably in space and that new steady state conditions can lag the climate change by tens of thousands of years. The results here suggest that environmental changes may also change the distribution of soil depth and PSD on the hillslope.

The model simulations analyzed in this paper employed a number of simplifying assumptions (outlined in section 2.3), allowing us to isolate and study causality between individual processes and drivers. The effects of these assumptions on simulated soil evolution are not yet known and will be investigated in future studies. Below, we provide our assessment of the implications of our assumptions in an attempt to frame the results of this study in the context of the overall soil evolution dynamics.

Topography–a temporally and spatially constant slope gradient was simulated. This prevented the development of a topographically heterogeneous slope profile (e.g., catena, concave, and convex) which can lead to changes in sediment transport rates along the hillslope. *Cohen et al.* [2010], using the mARM3D model, showed

that the shape of the hillslope profile will only significantly affect soil distribution for extreme cases. The results of the slope sensitivity analysis in the current paper (section 3.1) suggest that the assumption of a constant slope is reasonable, especially for steep slopes. For example, the equilibrium soil depth in the 30% simulation averages 61 cm for the upper half and 37 cm for the bottom half of the hillslope. This means that the maximum potential change of gradient for our 100 m long hillslope is (0.61–0.37)/100 which is less 0.003 m/m, which in turn is less than a 1% change in the gradient of the hillslope over the duration of the simulation. Moreover, *Sharmeen and Willgoose* [2007] and *Willgoose and Sharmeen* [2006] showed that a constant slope does not significantly affect accuracy of results since soils typically evolve faster than landforms, and soils are thus in equilibrium with the evolving landform. We thus conclude that changes in soil depth dominate changes in hillslope topography and gradient at the time scales of our simulations and that our computational approximation of an evolving soil on a fixed landform is satisfactory for the purpose of this paper. That being said, the interaction between landform and soil evolution (often referred to as soil-landscape evolution) is interesting particularly considering that soil-landscape evolution modeling is an emerging field in geomorphology [e.g., *Minasny and McBratney*, 2006; *Vanwalleghem et al.*, 2013].

Soil profile PSD–the assumption of a perfectly mixed profile layer reduces the potential graduality in soil profile distribution. This is a very commonly used assumption for aerial representation of a landscape using a grid mesh. Some soil profile models [e.g., *Yoo and Mudd*, 2008b] use dynamic profile layer size. Our algorithmic solution of constant layer size is largely dictated by computational efficiency which led us to our use of transition matrices to describe the 3-D soil-landscape (see *Cohen et al.* [2009, 2010]] for more details). Biological and chemical soil profile processes can significantly affect soil profile PSD in some regions. For example, landscapes subject to intense burrowing activity (e.g., by moles and gophers) are subject to rapid soil mixing, yielding a very different soil profile PSD from that predicted in this paper.

Soil hydrology–soil hydrological properties and runoff generation processes are assumed in our model to be constant in space and time. Overland flow dynamics can, however, considerably change as a function of both soil properties and vegetation dynamics [*Abrahams et al.*, 1995; *Assouline and Ben-Hur*, 2006; *Chen et al.*, 2013], which will, in turn, affect runoff and sediment transport rates.

Soil geomorphology–soil chemistry and biology (e.g., clay aggregation and biological crust) can affect the susceptibility of the soil surface to erosion [*Belnap*, 2006]. More research is needed to quantify these small-scale dynamics in the context of large-scale soil-landscape evolution. While more sophisticated assumptions can be used to incorporate these soil characteristics, simulating them at landscape and even hillslope scales will be highly challenging.

Climatic and anthropogenic drivers–when considering long-term soil evolution, it is likely that climatic and other environmental characteristics will change or fluctuate, with significant implication for the resulting soil scape. In semiarid environments, for example, changes in storm intensity and timing over millennial time scales may have a significant effect on soil erosion rates. Lumping interannual precipitation patterns (as done here) may also lead to considerably different erosion rates, especially in relatively arid climatic regimes where few high-intensity rainfall storms can be responsible for the majority of the annual catchment sediment yield [*Nearing et al.*, 2007].

Soil production–soil production by weathering was assumed to vary only as a function of in situ soil depth. Considering more complex dynamics (e.g., as a function of microclimate) can yield a more diverse soil distribution, particularly (and arguably) for chemical and biologically driven weathering processes [e.g., *Yoo and Mudd*, 2008a].

Aeolian transport–aeolian sediment transport is a very complex and dynamic process. Sediment accumulating dynamics on the landscape can vary at both macroscale and microscale [*Fearnehough et al.*, 1998]. Temporal changes in accumulation and erosion rates may also be significant [*Pelletier*, 2007]. These factors should be considered when assessing the soil evolution of a real, aeolian-dominated landscape. The temporal factor is likely to be particularly important given that many aeolian-driven soilscapes are no longer under a significantly active aeolian regime (e.g., the European Loess Belt). The effects of temporal fluctuations in aeolian accumulation rates will be studied in a subsequent paper.

5. Conclusions

We developed and applied a new numerical model to study the potential effect of aeolian soil development on soil evolution. We identified key differences between aeolian-driven and bedrock-weathering soil

production: absence in the former of (1) surface armoring, (2) soil production depth dependency, and (3) particle size distribution (PSD) self-organization. We tested the potential effects of these differences using a set of simulations employing different sediment transport mechanisms (fluvial or diffusive), soil supply source (bedrock or aeolian), and sediment PSD (coarse- or fine-grained aeolian deposition).

The results show that surface armoring plays a major role in soil evolution. By reducing soil erosion and in combination with a depth-dependent soil production, armoring stabilizes the soil, leading to a steady state soil grading and depth. The spatial variability in soil depth and soil profile PSD is also strongly driven by the formation of a surface armor. Under an aeolian soil production regime or when sediment transport of soil is not impacted by surface PSD (i.e., diffusion in our model), the spatial variability of steady state soil distribution was considerably higher. We propose that this may help explain the patchy soil distribution that is often observed in aeolian-dominated regions. This points to potential soil distribution patterns resulting from different soil production and transport regimes. While the simulations we used in this analysis are a simplified expression of the soil process and dynamics, these signals are potentially indicative of behavior in natural landscapes. Further study is needed to better constrain and model this process.

For aeolian-dominated conditions, we consequently propose that different parts of the hillslope will be either erosional or depositional; the transition between these two modes will not be gradual but subject to a threshold conditioning. We further propose that the absence of a stabilizing armor layer will lead to a soil which is more responsive to environmental change (e.g., climate and land use). This is because changes may lead to spatially variable mode shifts.

The differences between aeolian and weathering soil production regimes were most pronounced for hillslopes that are dominated by fluvial sediment transport. Under the aeolian regime, even if a coarse surface layer forms, fresh fine sediment will be deposited on top of this surface layer thus inhibiting armor formation. Since diffusive transport (as modeled here) is not affected by surface PSD, the differences between the soil production regimes were relatively small for diffusive-dominated hillslopes. Given that our results show that different parts of the hillslope tend to be dominated by either diffusive or fluvial processes, we propose that aeolian-dominated landscapes or periods of increased aeolian input can potentially have very different soil evolution and with potentially considerable spatial variability at the landscape and hillslope scales.

Acknowledgments

This research was supported, in part, by the Israel Science Foundation (grant 1184/11). G.R.W. was supported by an Australian Research Council Australian Professorial Fellowship. We would like to thank Nicole Gasparini and three reviewers for their insightful and useful comments. Model code and input data are freely avalible on the Community Surface Dynamics Modeling System model repository: http://csdms.colorado.edu/wiki/Model_portal.

References

Abrahams, A. D., A. J. Parsons, and J. Wainwright (1995), Effects of vegetation change on interrill runoff and erosion, Walnut Gulch, Southern Arizona, *Geomorphology*, *13*(1), 37–48.

Ahnert, F. (1976), Brief description of a comprehensive three-dimensional process-response model for landform development, *Z. Geomorphol., N.F. Supplement 25*, 29–49.

Ahnert, F. (1977), Some comments on the quantitative formulation of geomorphological process in a theoretical model, *Earth Surf. Process.*, *2*, 191–201.

Assouline, S., and A. Ben-Hur (2006), Effects of rainfall intensity and slope gradient on the dynamics of interrill erosion during soil surface sealing, *Catena*, *66*(3), 211–220, doi:10.1016/j.catena.2006.02.005.

Belnap, J. (2006), The potential roles of biological soil crusts in dryland hydrologic cycles, *Hydrol. Process.*, *20*(15), 3159–3178, doi:10.1002/hyp.6325.

Bruins, H. J., and D. H. Yaalon (1992), Parallel advance of slopes in aeolian loess deposits of the northern Negev, Israel, *Isr. J. Earth Sci.*, *41*, 189–199.

Carson, M. A., and M. J. Kirkby (1972), *Hillslope Form and Process*, pp. 475, Cambridge Univ. Press, Cambridge, U.K.

Chen, L., S. Sela, T. Svoray, and S. Assouline (2013), The role of soil-surface sealing, microtopography, and vegetation patches in rainfall-runoff processes in semiarid areas, *Water Resour. Res.*, *49*(9), 5585–5599, doi:10.1002/wrcr.20360.

Cohen, S., G. Willgoose, and G. Hancock (2009), The mARM spatially distributed soil evolution model: A computationally efficient modeling framework and analysis of hillslope soil surface organization, *J. Geophys. Res.*, *114*, F03001, doi:10.1029/2008JF001214.

Cohen, S., G. Willgoose, and G. Hancock (2010), The mARM3D spatially distributed soil evolution model: Three-dimensional model framework and analysis of hillslope and landform responses, *J. Geophys. Res.*, *115*, F04013, doi:10.1029/2009JF001536.

Cohen, S., G. Willgoose, and G. Hancock (2013), Soil-landscape response to mid and late Quaternary climate fluctuations based on numerical simulations, *Quat. Res.*, *79*(3), 452–457, doi:10.1016/j.yqres.2013.01.001.

Crouvi, O., J. D. Pelletier, and C. Rasmussen (2013), Predicting the thickness and aeolian fraction of soils in upland watersheds of the Mojave Desert, *Geoderma*, *195*, 94–110, doi:10.1016/j.geoderma.2012.11.015.

Culling, W. E. H. (1963), Soil creep and the development of hillside slopes, *J. Geol.*, *71*(2), 127–161.

Eldridge, D. J., E. Zaady, and M. Shachak (2002), Microphytic crusts, shrub patches, and water harvesting in the Negev Desert: The Shikim system, *Landscape Ecol.*, *17*(6), 587–597.

Engelhund, F., and E. Hansen (1968), *A Monograph on Sediment Transport in Alluvial Streams*, pp. 62, Teknish Forlag, Technical Press, Copenhagen, Denmark.

Fearnehough, W., M. Fullen, D. Mitchell, I. Trueman, and J. Zhang (1998), Aeolian deposition and its effect on soil and vegetation changes on stabilised desert dunes in northern China, *Geomorphology*, *23*(2–4), 171–182, doi:10.1016/S0169-555X(97)00111-6.

Fleming, R. W., and A. M. Johnson (1975), Rates of seasonal creep of silty clay soil, *Q. J. Eng. Geol.*, *8*, 1–29.

Gilbert, G. K. (1877), *Report of the Henry Mountains (Utah), U.S. Geographical and Geological Survey of Rocky Mountains Region*, pp. 169, U.S. Gov. Print. Off., Washington, D. C.
Henderson, F. M. (1966), *Open Channel Flow*, MacMillan, New York.
Heimsath, A. M., W. E. Dietrich, K. Nishiizumi, and R. C. Finkel (1997), The soil production function and landscape equilibrium, *Nature*, *388*(6640), 358–361.
Hillel, D. (1982), *Introduction to Soil Physics*, pp. 364, Academic Press Inc., London.
Hughes, M. W., J. Schmidt, and P. C. Almond (2009), Automatic landform stratification and environmental correlation for modeling loess landscape in North Otago, South Island, New Zealand, *Geoderma*, *149*, 92–100.
Hughes, M. W., P. C. Almond, J. J. Roering, and P. J. Tonkin (2010), Late Quaternary loess landscape evolution on an active tectonic margin, Charwell Basin, South Island, New Zealand, *Geomorphology*, *122*, 294–308.
Kim, J., and V. Y. Ivanov (2014), On the nonuniqueness of sediment yield at the catchment scale: The effects of soil antecedent conditions and surface shield, *Water Resour. Res.*, *50*, 1025–1045, doi:10.1002/2013WR014580.
McFadden, L. D., and P. L. K. Knuepfer (1990), Soil geomorphology: The linkage of pedology and superficial processes, edited by P.L.K. Knuepfer and L.D. MacFadden, Soils and Landscape Evolution, *Geomorphology*, *3*, 197–205.
Minasny, B., and A. B. McBratney (2006), Mechanistic soil-landscape modeling as an approach to developing pedogenesis classifications, *Geoderma*, *133*, 138–149.
Nearing, M. A., M. H. Nichols, J. J. Stone, K. G. Renard, and J. R. Simanton (2007), Sediment yields from unit-source semiarid watersheds at Walnut Gulch, *Water Resour. Res.*, *43*, W06426, doi:10.1029/2006WR005692.
O'Callaghan, J. F., and D. M. Mark (1984), The extraction of drainage networks from digital elevation data, *Comput. Vision, Graphics, Image Process.*, *28*(3), 323–344, doi:10.1016/S0734-189X(84)80011-0.
Pelletier, J. D. (2007), Cantor set model of eolian dust deposits on desert alluvial fan terraces, *Geology*, *35*(5), 439–442, doi:10.1130/G23367A.1.
Pelletier, J. D. (2008), *Quantitative Modeling of Earth Surface Processes*, pp. 295, Cambridge Univ. Press, Cambridge, U. K.
Pelletier, J. D., et al. (2011), Calibration and testing of upland hillslope evolution models in a dated landscape: Banco Bonito, New Mexico, *J. Geophys. Res.*, *116*, F04004, doi:10.1029/2011JF001976.
Roering, J. J. (2004), Soil creep and convex-upward velocity profiles: Theoretical and experimental investigation of disturbance-driven sediment transport on hillslopes, *Earth Surf. Processes Landforms*, *29*(13), 1597–1612.
Roering, J. J. (2008), How well can hillslope evolution models "explain" topography? Simulating soil transport and production with high-resolution topographic data, *Geol. Soc. Am. Bull.*, *120*(9–10), 1248–1262.
Sela, S., T. Svoray, and S. Assouline (2012), Soil water content variability at the hillslope scale: Impact of surface sealing, *Water Resour. Res.*, *48*, W03522, doi:10.1029/2011WR011297.
Sharmeen, S., and G. R. Willgoose (2006), The interaction between armoring and particle weathering for eroding landscapes, *Earth Surf. Processes Landforms*, *31*, 1195–1210, doi:10.1002/esp.1397.
Sharmeen, S., and G. R. Willgoose (2007), A one-dimensional model for simulating armouring and erosion on hillslopes: 2. Long term erosion and armouring predictions for two contrasting mine spoils, *Earth Surf. Processes Landforms*, *32*, 1437–1453, doi:10.1002/esp.1482.
Vanwalleghem, T., U. Stockmann, B. Minasny, and A. B. McBratney (2013), A quantitative model for integrating landscape evolution and soil formation, *J. Geophys. Res. Earth Surf.*, *118*, 331–347, doi:10.1029/2011jf002296.
Wells, T., G. R. Willgoose, and G. R. Hancock (2008), Modeling weathering pathways and processes of the fragmentation of salt weathered quartz-chlorite schist, *J. Geophys. Res.*, *113*, F01014, doi:10.1029/2006JF000714.
Willgoose, G. R., and S. Sharmeen (2006), A one-dimensional model for simulating armoring and erosion on hillslopes: I. Model development and event-scale dynamics, *Earth Surf. Processes Landforms*, *31*, 970–991.
Yair, A., and A. Kossovsky (2002), Climate and surface properties: Hydrological response of small and and semi-arid watersheds, *Geomorphology*, *42*(1–2), 43–57.
Yoo, K., and S. M. Mudd (2008a), Discrepancy between mineral residence time and soil age: Implications for the interpretation of chemical weathering rates, *Geology*, *36*(1), 35–38.
Yoo, K., and S. M. Mudd (2008b), Toward process-based modeling of geochemical soil formation across diverse landforms: A new mathematical framework, *Geoderma*, *146*(1–2), 248–260.